2013 IEEE International Conference on Robotics and Automation (ICRA)
Karlsruhe, Germany, May 6-10, 2013

Motion Estimation of Snake Robots in Straight Pipes

Florian Enner, David Rollinson and Howie Choset

***Abstract*— We present a method of estimating a snake robot's motion inside and outside of straight pipes using only knowledge of the robot's joint angles. We accomplish this by introducing a novel method to constructing a body frame for the robot that is aligned with the centerline of the pipe. In addition to greatly simplifying the motion model this method allows us to accurately estimate the diameter of the pipe. We present experimental results using a 16-DOF snake robot traversing the inside and outside of straight pipes.**

I. Introduction

Snake robots have a wide range of potential applications in pipes providing inspection with visual sensing and other non-destructive testing (NDT) sensors. Accurately modeling the motion of the robot is critical to developing these robots into robust inspection and work platforms. Over the years, our lab has developed snake robots [1] controlled by parameterized cyclic motions (gaits) [2] that can locomote on both the inside and outside of pipes of a range of different diameters. This work leverages the unique locomotive properties of the robot and the *pipe crawling* and *pole climbing* gaits (Fig. 1) to construct a motion model that estimates not only the robot's motion, but the geometry of the pipe as well. Determining pipe geometry purely from the locomotion of the robot is unique since this can allow one to estimate the amount of corrosion or build-up in a pipe even if visual or external sensing is not possible.

In this paper we present two novel contributions. The first is that we extend a previously developed motion model for snake robots on flat ground [3] to cylindrical pipes and poles. This model is made possible by using a body frame for the robot that is aligned with centerline of the pipe, greatly simplifying the analysis of the robot's motion. Our second contribution lies in calculating this body frame in real-time, using the known structure of the robot's gait. Previously determining this body frame required off-line calculation and lookup tables that covered a limited range of the robot's gait parameter space.

All experiments in this work have been done with a 16-DOF snake robot. Different configurations do not have a significant impact on the mentioned gaits as long as the robot is long enough to wrap around the object approximately 1.5 times to be properly aligned and short enough to not exceed power limitations. Experiments demonstrating this approach are provided in an accompanying video

Florian Enner is a staff researcher in the Robotics Institute, Carnegie Mellon University, Pittsburgh, PA, 15213 enner@cmu.edu
David Rollinson is a graduate student in the Robotics Institute, Carnegie Mellon University, Pittsburgh, PA, 15213 drollins@cs.cmu.edu
Howie Choset is a professor in the Robotics Institute, Carnegie Mellon University, Pittsburgh, PA, 15213 choset@cmu.edu

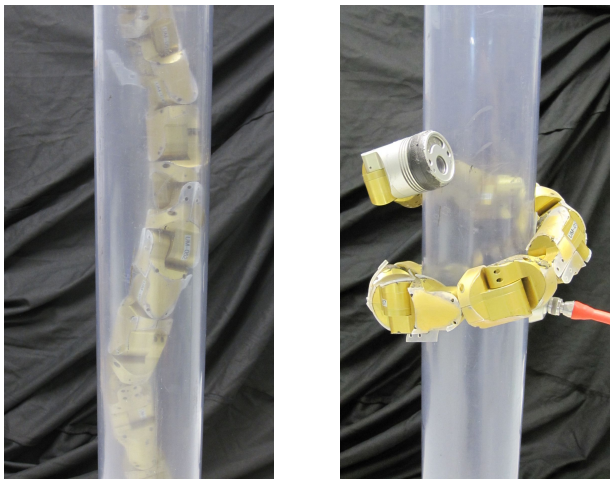

(a) pipe crawling (b) pole climbing

Fig. 1: Examples of a snake robot executing pipe crawling (a) and pole climbing (b).

II. Prior Work

Prior work exists on using snake-like robots in pipes. Kuwade et al [4] use a robot with a piece-wise two-dimensional gait to negotiate bends and junctions in pipe. While the robot can adapt to different diameters internally, they do not estimate the robot's motion down the pipe in straight sections, nor can they locomote at all on the outside of pipes. Other wheeled snake robots have been developed specifically for internal pipe inspection [5], [6] [7]. While the motion of these robots is much simpler to analyze, they operate only in tight ranges of pipe diameters. Our snake robots have successfully climbed the insides and outsides of pipes ranging from 7.5 to 30 cm (3 to 12 inches) in diameter [2].

To the best of our knowledge there exists no previous work in modeling the motion of snake robots inside or on pipes. However, there is existing work in modeling the motion of biological snakes [8], [9] and robotic snakes [10], [11] on flat ground. Recently we developed a motion model for this domain [3] that differs from existing approaches in that we do not rely on complex modeling of friction and ground contact. Instead, we leverage the separation of internal and external motion provided by using the virtual chassis body frame [12].

III. Pipe Climbing Gait and Robot Kinematics

To coordinate the many degrees of freedom (DOF) in our snake robots, we rely on lower-dimensional parameterized gait functions [2]. Since our robots consist of single-DOF

978-1-4673-5643-5/13/$31.00 ©2013 IEEE

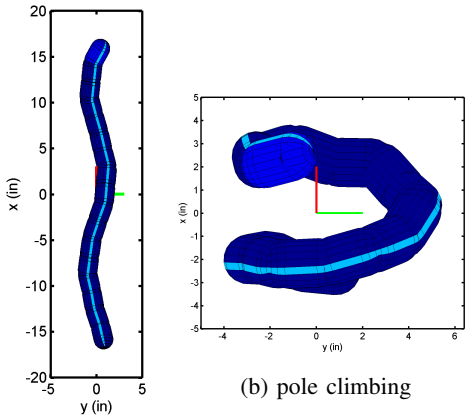

(a) pipe crawling

(b) pole climbing

Fig. 2: Examples of the gaits discussed in this work represented in the virtual chassis body frame. Pipe crawling (a) and pole climbing (b).

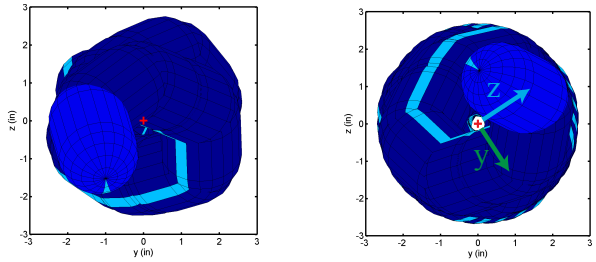

(a) 16 modules

(b) 200 modules

Fig. 3: Top view of the virtual chassis body frame computed for a 16-DOF (a) and a 200-DOF (b) snake robot. The centerline found by SVD in higher DOF systems is much better aligned with the true centerline of the shape generated by the pole climbing gait. The ambiguous z-axis is defined to point towards the centerpoint of the first module.

modules oriented alternately in the lateral and dorsal axes [1], our gait equations consist of separate functions for each axis. The pipe crawling and pole climbing gaits are different parameterizations of the rolling helix gait

$$\bar{\theta}(t) = \begin{cases} A{\cdot}\sin(\xi) & \text{odd} \\ A{\cdot}\sin(\xi + \frac{\pi}{2}) & \text{even} \end{cases} \quad (1)$$

$$\xi = \omega t + \nu n. \quad (2)$$

The spatial frequency ν and amplitude A are analogous to the Frenet-Serret torsion [13] and curvature of the helical backbone shape respectively. The overall cylindrical helix generated by the pipe crawling and pole climbing gaits remain constant through the gait cycle. The temporal position within the gait controls how the modules are rotated along this shape, and is controlled by ωt in (2). Pipe crawling is a parametrization of a helix in which ν is set to 0.095 for a 16-link robot. In pole climbing ν is set to 0.015.

IV. Virtual Chassis Body Frame

The virtual chassis is a body frame for snake robots that is constantly aligned with the principal components of the robot's overall shape. We have observed that this body frame can approximately separate a robot's internal shapes changes from its external motion in world. For shapes that have distinct principal components, the virtual chassis can easily be calculated using singular value decomposition (SVD) [14]. However, for shapes generated by the pole climbing gait the axis corresponding to the first principal component is not necessarily aligned with the true centerline of the helix, as seen in Fig. 2, especially for snake robots that have few modules. Previously, this was addressed by using non-linear optimization techniques to align the virtual chassis with the true centerline of the robot's helical shape. However, this optimization was slow, requiring offline calculation and lookup tables based on estimated gait parameters to run in real time. Additionally, in this gait the second and third moments of inertia are ambiguous, thus causing problems when calculating the virtual chassis with SVD.

To perform online computation of the virtual chassis for snake robots in and on pipes, we estimate the gait parameters of the robot's shape and generate an idealized snake robot of 'infinite' length where the first principle moment of inertia is identical to the true centerline of the robot's helical shape. These gait parameters are fit at every time step by an EKF, similar to one that was presented previously [14]. Using these parameters and the forward kinematics corresponding to the gait equation (1) we can generate a snake robot of arbitrary length. In practice, a length of 200 modules is sufficient to approximate the desired effect, as illustrated in Fig. 3.

The positive x-axis is then defined to be aligned with the centerline of the robot's helical shape pointing towards the front of the robot. Similar to the optimization procedure in [12], the robot is oriented around the centerline by defining the positive z-axis to point towards the centerpoint of the head module. The y-axis follows the right hand rule.

A 16-module subset of this 'infinite snake' is selected that represents an 'idealized' (no position errors) snake of the same length as the robot. The forward kinematics of the real snake robot are then fit to this idealized shape to define its virtual chassis.

V. Motion Model

In this section, we describe our mathematical model that estimates world motion of a snake robot on the inside and outside of pipes. A modified version of the virtual chassis [12] based on gait parameter estimation [14] is computed at every time step to provide a body frame that allows us to better observe the motion of a robot's modules with respect to the world. This body frame has the additional benefit that the x-axis is defined to align with the centerline of the robot's helical shape, and by assumption the centerline of the pipe. We exploit this property to estimate the diameter of the pipe, the points of contact between the robot and the pipe, and the resulting world motion of the snake robot.

We assume a no slip condition, which means that the contact point is instantaneously stationary in the world frame. As a result, we can compute the motion of a module in

the body frame and then conclude that the motion in the body frame and the world frame are opposite, allowing us to approximate world motion by averaging the contribution of each module.

A. Estimating the Pipe Radius

Analyzing the shape of the robot allows for the radius of the pipe to be estimated in real time. This can provide valuable information for pipe inspection, since the robot could be able to estimate and localize the amount of buildup and corrosion. Buildup and corrosion can cause severe problems that cannot be seen from the outside of a pipe, but result in variations of the inner pipe radius. Furthermore using the snake robot, these measurements could be made even when internal visual inspection and other forms of NDT are not possible.

In an idealized pipe, the distance between the centerline of the pipe and a module's center is the same for each module. By averaging the distances from the x-axis of the body frame to the center of each module, we can reduce the noise induced by using a real system

$$\rho_t = \frac{1}{n}\sum_{i=1}^{n} \| \begin{bmatrix} y^i \\ z^i \end{bmatrix}_t \|. \tag{3}$$

In (3), ρ_t is the average distance between all modules and the x-axis, which is aligned with the centerline of straight pipes, at time t. Deviations from the average distance for single modules can indicate irregularities in the pipe radius caused by corrosion or deposits.

The pipe radius r additionally depends on the distance between the center of a module and the true contacting point,

$$r_t = \rho_t \pm \frac{d}{2}. \tag{4}$$

We approximate the distance from a module's center to the contact point by modeling the module as a sphere with diameter d (equal to the diameter of a module), as shown in figure 4. When using the robot outside of a pipe, the radius of the spherical module in (4) needs to be subtracted instead of added.

B. Module Motion

Motion through the world can be caused by two types of motion of modules in contact with the pipe. First, a rotation about a module's center can induce motion in a manner similar to a wheel. Second, a translation of a module's center with respect to the virtual chassis body frame can induce world motion in a manner similar to a person walking. Both types of motion are illustrated in figure 5. Due to the fixed overall shape of 'rolling'-type gaits, the translational component is almost non-existent for pipe crawling and pole climbing. However, we include both types of motion in our model to not limit ourselves to the specifics of these particular gaits.

First, we calculate the translational component of a module's motion by looking at the differential position changes

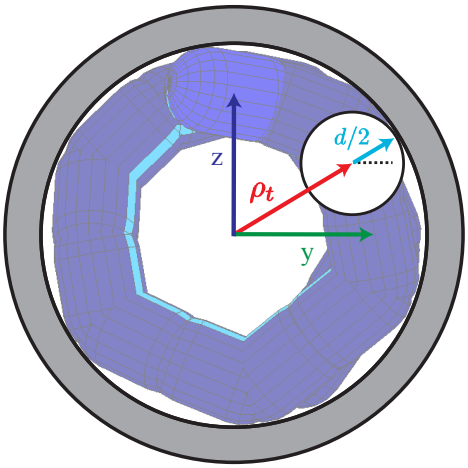

Fig. 4: Illustration of a simple way to estimate the diameter of pipes. The pipe radius is equal to the distance of a module's center from the x-axis in the virtual chassis body frame ρ_t plus the radius of the module $\frac{d}{2}$.

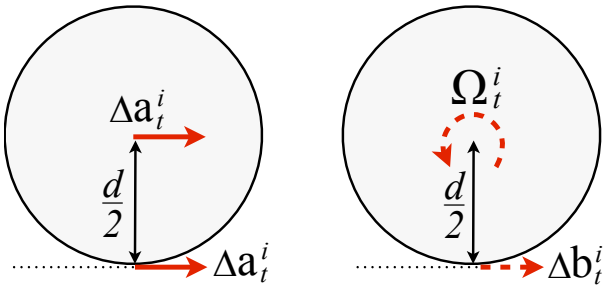

Fig. 5: A 2-D representation of the cross section of a module's sphere of contact and the effects of translation and rotation on the point that is assumed to be in contact with the pipe.

between time steps. The position of the ith module's center in the virtual chassis body frame at time t is,

$$\mathbf{a}_t^i = \begin{bmatrix} x^i \\ y^i \\ z^i \end{bmatrix}_t. \tag{5}$$

Thus, the differential translation of the ith module in the virtual chassis body frame at time t is

$$\Delta\mathbf{a}_t^i = \mathbf{a}_t^i - \mathbf{a}_{t-1}^i. \tag{6}$$

To calculate the world motion induced by rotation about a module's center, we must first determine the point of contact between the module and the pipe. This can be achieved using logic similar to that used in pipe radius estimation. We find the direction $\mathbf{s}_t^i$ of the point of contact of a module in the yz-plane of the virtual chassis body frame,

$$\mathbf{s}_t^i = \pm \frac{\begin{bmatrix} y^i \\ z^i \end{bmatrix}_t}{\| \begin{bmatrix} y^i \\ z^i \end{bmatrix}_t \|} \tag{7}$$

In the second step, we construct a vector oriented in $\mathbf{s}_t^i$ ($-\mathbf{s}_t^i$ for the outside of a pipe) that has a length equivalent to the radius of the approximate sphere of contact $\frac{d}{2}$. The

resulting vector is then rotated into the local frame of module i at time t in order to compute angular velocities more easily,

$$\mathbf{q}_t^i = (\mathbf{R}_t^i)^{-1} \begin{bmatrix} 0 \\ \frac{d}{2}\mathbf{s}_t^i \end{bmatrix}. \tag{8}$$

In (8) $\mathbf{R}_t^i$ is the rotation matrix that describes the orientation of the ith module in the body frame at time t.

The differential rotation in the ith module's frame between time t and $t-1$ can be determined by

$$\mathbf{\Omega}_t^i = (\mathbf{R}_{t-1}^i)^{-1}\mathbf{R}_t^i. \tag{9}$$

To even out non-linearities, we apply the differential rotation $\mathbf{\Omega}_t^i$ both forwards and backwards to the point of contact $\mathbf{q}_t^i$, average the displacements induced by rotational motion, and rotate the result back into the virtual chassis body frame,

$$\Delta\mathbf{b}_t^i = \mathbf{R}_t^i \frac{\mathbf{\Omega}_t^i\mathbf{q}_t^i - (\mathbf{\Omega}_t^i)^{-1}\mathbf{q}_t^i}{2}. \tag{10}$$

Finally, the sum of the motion components that are induced by module translation $\Delta\mathbf{a}_t^i$ and module rotation $\Delta\mathbf{b}_t^i$ results in the module's total motion $\Delta\mathbf{p}_t^i$,

$$\Delta\mathbf{p}_t^i = \Delta\mathbf{a}_t^i + \Delta\mathbf{b}_t^i. \tag{11}$$

C. Body Frame Translation

Assuming that all modules are in equal contact with the pipe, we can estimate the overall translation of the body frame with respect to the world by averaging the reactive differential motions of all modules at time t,

$$\Delta\mathbf{m}_t = -\frac{1}{n}\sum_{i=1}^{n}\Delta\mathbf{p}_t^i. \tag{12}$$

Our simple assumption of equal ground contacts can easily be interchanged to other models or measurements of ground contact forces by weighting each module's motion separately.

D. Body Frame Rotation

The rotational motion of the body frame can be calculated in a similar manner as translation. Because environmental constraints within pipes only allow rotation about the centerline (which corresponds to the x-axis) we can simply combine the rotational effects of each module. For this, we form a moment vector by calculating the cross product of each module's position in the virtual chassis frame with the x-axis and then normalize the results,

$$\mathbf{d}_t^i = \begin{bmatrix} 1 \\ 0 \\ 0 \end{bmatrix} \times \mathbf{a}_t^i \tag{13}$$

$$\bar{\mathbf{d}}_t^i = \frac{\mathbf{d}_t^i}{\|\mathbf{d}_t^i\|}. \tag{14}$$

We then compute the differential angle of rotation of the body frame $\Delta\theta_t$ by averaging the dot products of the moment and motion vectors corresponding to each module,

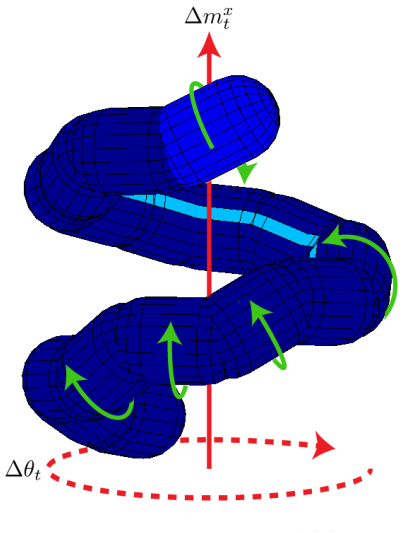

Fig. 6: Diagram showing the estimated world motion by averaging the motion of each module.

and dividing the result by the distance to the centerline, which is equal to the pipe radius r_t,

$$\Delta\theta_t = -\frac{1}{r_t n}\sum_{i=1}^{n}\Delta\mathbf{p}_t^i \cdot \bar{\mathbf{d}}_t^i. \tag{15}$$

The result in (15) is the negation of the rotational motion of the modules because of the reactive movement that a module induces in the world.

E. Full Body Frame Motion

The rotational and translational components of world motion (at time t) can be combined into a single transform matrix that can easily update the world position of the virtual chassis body frame,

$$\mathbf{T}_t = \begin{bmatrix} 1 & 0 & 0 & \Delta m_t^x \\ 0 & \cos(\Delta\theta_t) & -\sin(\Delta\theta_t) & 0 \\ 0 & \sin(\Delta\theta_t) & \cos(\Delta\theta_t) & 0 \\ 0 & 0 & 0 & 1 \end{bmatrix}. \tag{16}$$

In (16) Δm_t^x is the x-component of the translational motion of the body frame at time t. The other components of Δm_t are omitted because pipes do not allow motion in the corresponding directions. An illustration of the resulting world motion using this method is shown in Fig. 6.

VI. Experiment

We performed experiments to measure the accuracy of our model while performing two gaits, i.e., pipe crawling and pole climbing. We conducted 6 trials of each gait, resulting in a total of 12 trials. Each trial was started at a different position in the gait cycle and traversed different distances and directions in order to sample a wide range of motion in the world. Pipe crawling trials were conducted in a horizontal pipe and pole climbing tests were done on a vertical pipe. We recorded the feedback joint angles from the robot and manually measured the traveled distance for each run. For

the trials, rotation about the centerline was not measured due to the difficulties of getting an accurate measurement.

Table I shows the mean errors for the predicted motions of both gaits traveling in both directions. We attribute the high error when climbing down the pole to gravitationally induced slippage. The estimated velocities during a trial of forward pipe crawling are shown in figure 7. Note that the EKF used for gait parameter estimation needs time to converge, which results in the errors seen at 2 seconds. Table II shows estimates of the average velocities about the centerline for both gaits and their average rotation per inch of forward travel. The velocity estimates approximately match the observed behavior in the real world. Note that the ratio of translation compared to rotation is much larger for the lower-pitched helix of the pole climbing gait relative to the higher-pitched helix used in pipe crawling.

Figure 8 shows our method to approximate the pipe radius computed on a test setup that combines pipes of varying diameters. The estimates of the main sections show accuracies within 0.1 inch.

VII. Conclusion

We have presented an effective way to model the motion of a non-wheeled snake robot on the inside and outside of straight pipes. Even though the assumptions of our model neglect dynamic effects like inertia or frictional forces, it provides a relatively accurate estimate of motion. Our method additionally provides a unique way to estimate the radius of a pipe in real time without the use of specialized sensors. Measuring pipe diameter allows for the detection and identification of pipe defects such as build-up or corrosion, even if visual or external sensing is not possible.

We have also presented a computationally efficient way to construct a specialized body frame for pipes that separates a snake robot's internal shape changes from its external motions through the world. This allows us to more intuitively represent and analyze the motion of the robot's modules with respect to the pipe environment in which the robot is traveling.

The most significant limitation of our current model is the assumption of straight pipes. This limitation also exists in the gait motions we have designed thus far. Both controlling and modeling the snake robot's motions through bends in pipes involves adding more shape modes and parameters to a gait. However, this creates new challenges because the geometric features of the robot's shape, which cause the first principal component to be aligned with the centerline of the pipe, are lost. Additionally, observing world motion becomes significantly more complex without a body frame that remains static with respect to the overall shape of the robot. Overcoming these are necessary to perform useful pipe inspections in the real world.

Perhaps the most relevant extension of this work would be the integration as a motion model in SLAM algorithms. In many ways the approximation of this model mirrors the no-slip assumption often made in the motion model of many wheeled robotic systems.

By combining this basic motion model with an estimate of the robot's pose [12], we have made initial progress in dead-reckoning a map of pipes based on the robot's motion. Future work will extend these techniques to take better advantage of the fact that the robot is long with respect to variations in the pipe diameter, and can thus iteratively map pipe from head to tail as it travels forwards.

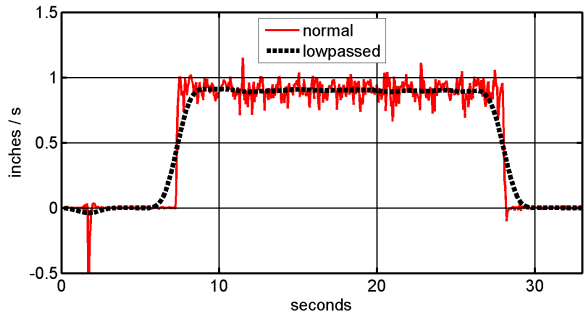

(a) estimated velocity

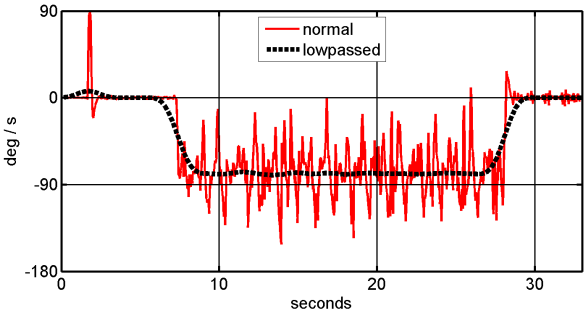

(b) estimated angular velocity

Fig. 7: Plot of the estimated translational velocity in the direction of the pipe (a) and the angular velocity about the centerline of the pipe (b). The average translation during operation is 0.9 inches per second at an average angular rotation of -80 degrees per second.

TABLE I: Estimation errors [%] of the translational motion of the body frame down the x-axis (aligned with the centerline of the pipe) relative to manual measurements. Pipe crawling trials were conducted in a horizontal pipe and pole climbing tests were done on a vertical pole. Each row represents averaged values of 3 trials.

	estimation error along the x-axis	
	Mean	Dev.
Pipe crawling front	+5 %	2 %
Pipe crawling back	+8 %	2 %
Pole climbing up	-3 %	8 %
Pole climbing down	-31%	1 %

TABLE II: Estimates for the velocity in the direction of the pipe, angular velocity about the centerline of the pipe and the average rotation per inch of forward travel for pipe crawling and pole climbing. Each row represents averaged values of 3 trials.

	velocities		rotation per distance
	in / s	deg / s	deg / in
Pipe crawling front	+0.9	-80	-90
Pipe crawling back	-0.9	+80	-90
Pole climbing up	+1.9	-10	-5
Pole climbing down	-2.0	+12	-6

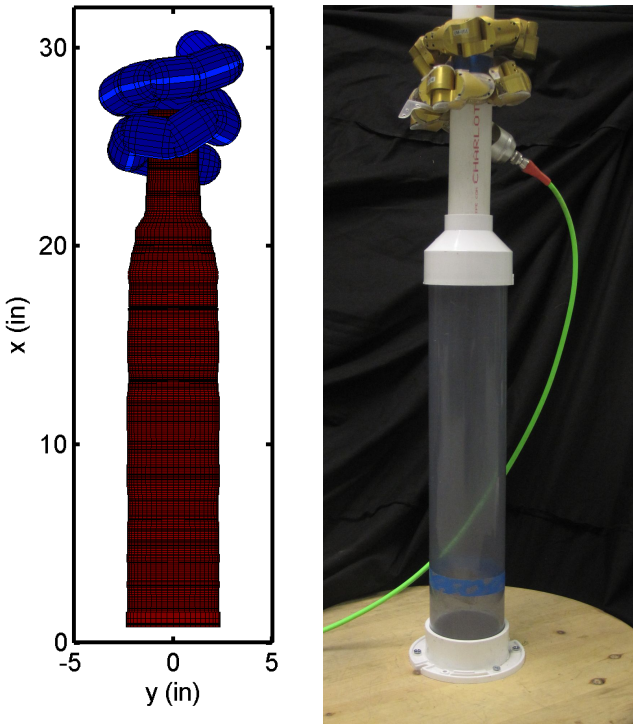

(a) Estimated outer diameter (b) Test setup

Fig. 8: Approximation of the outer diameter (a) of test setup (b), estimated at every timestep.

VIII. Acknowledgements

The authors would like to thank the members of the Biorobotics Lab and Robotics Institute, particularly Nico Zevallos, Matt Tesch and Glenn Wagner.

References

[1] C. Wright, A. Buchan, B. Brown, J. Geist, M. Schwerin, D. Rollinson, M. Tesch, and H. Choset, "Design and Architecture of the Unified Modular Snake Robot," in *IEEE International Conference on Robotics and Automation (accepted)*, 2012.

[2] M. Tesch, K. Lipkin, I. Brown, R. L. Hatton, A. Peck, J. Rembisz, and H. Choset, "Parameterized and Scripted Gaits for Modular Snake Robots," *Advanced Robotics*, vol. 23, pp. 1131–1158, June 2009.

[3] F. Enner, D. Rollinson, and H. Choset, "Simplified Motion Modeling for Snake Robots," in *International Conference on Robotics and Automation*, pp. 4216 – 4221, IEEE, 2012.

[4] A. Kuwada, S. Wakimoto, K. Suzumori, and Y. Adomi, "Automatic pipe negotiation control for snake-like robot," *2008 IEEE/ASME International Conference on Advanced Intelligent Mechatronics*, pp. 558–563, July 2008.

[5] H. Choi, S. Ryew, and S. Cho, "Development of Articulated Robot for Inspection of Underground Pipelines," in *International Conference on Structural Mechanics in Reactor Technology*, (Seoul, Korea), pp. 407–414, 1999.

[6] Z. Wang, Q. Cao, N. Luan, and L. Zhang, "Development of an autonomous in-pipe robot for offshore pipeline maintenance," *Industrial Robot: An International Journal*, vol. 37, no. 2, pp. 177–184, 2010.

[7] H. Schempf and E. Mutschler, "Visual and nondestructive evaluation inspection of live gas mains using the Explorer family of pipe robots," *Journal of Field Robotics*, vol. 33, pp. 217–249, 2010.

[8] D. I. Goldman and D. L. Hu, "The mechanics of slithering locomotion depend on the surroundings," *American Scientist*, pp. 314–323, 2010.

[9] Z. V. Guo and L. Mahadevan, "Limbless undulatory propulsion on land.," *Proceedings of the National Academy of Sciences of the United States of America*, vol. 105, pp. 3179–84, Mar. 2008.

[10] A. Transeth, R. Leine, C. Glocker, and K. Pettersen, "3-D Snake Robot Motion: Nonsmooth Modeling, Simulations, and Experiments," *IEEE Transactions on Robotics*, vol. 24, pp. 361–376, Apr. 2008.

[11] A. A. Transeth, R. I. Leine, C. Glocker, K. Y. Pettersen, and P. l. LiljebÄck, "Snake Robot Obstacle-Aided Locomotion: Modeling, Simulations, and Experiments," *IEEE Transactions on Robotics*, vol. 24, pp. 88–104, Feb. 2008.

[12] D. Rollinson and H. Choset, "Virtual Chassis for Snake Robots," in *IEEE International Conference on Intelligent Robots and Systems*, pp. 221 – 226, 2011.

[13] H. Yamada and S. Hirose, "Study on the 3d shape of active cord mechanism," *Robotics and Automation (ICRA)*, pp. 2890–2895, 2006.

[14] D. Rollinson, A. Buchan, and H. Choset, "State Estimation for Snake Robots," *IEEE International Conference on Intelligent Robots and Systems*, 2011.